Integrative Biology

Quantitative biosciences from nano to macro
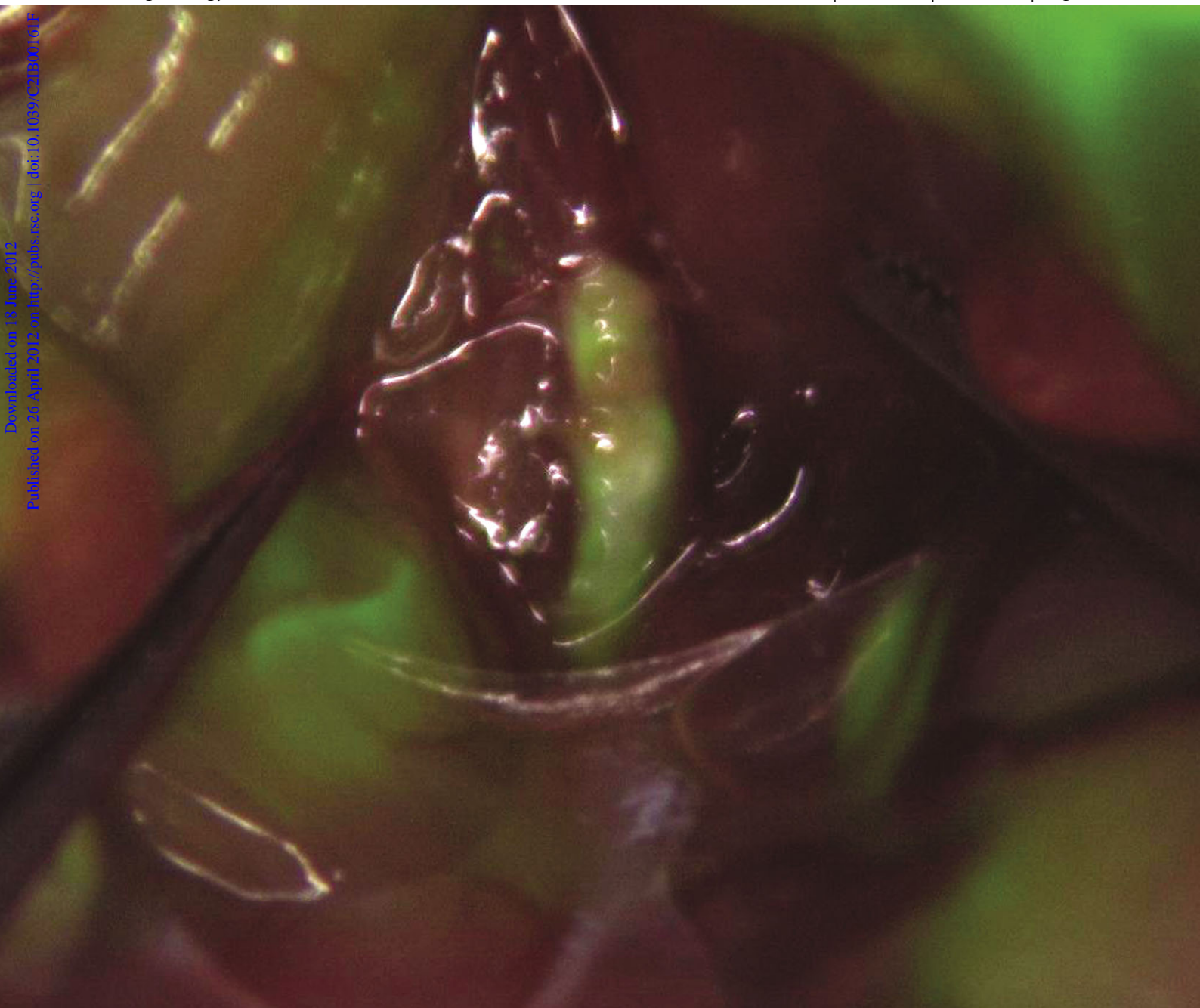
RSC Publishing

PAPER
Nguyen *et al.*
In vivo fluorescence imaging of atherosclerotic plaques with activatable cell-penetrating peptides targeting thrombin activity

PAPER

In vivo fluorescence imaging of atherosclerotic plaques with activatable cell-penetrating peptides targeting thrombin activity†

Emilia S. Olson,[ab] Michael A. Whitney,[a] Beth Friedman,[a] Todd A. Aguilera,[ab]
Jessica L. Crisp,[c] Fred M. Baik,[d] Tao Jiang,[e] Stephen M. Baird,[f]
Sotirios Tsimikas,[g] Roger Y. Tsien[ae] and Quyen T. Nguyen*[h]

Thrombin and other coagulation enzymes have been shown to be important during atherosclerotic disease development. Study of these proteases is currently limited because of lack of robust molecular imaging agents for imaging protease activity *in vivo*. Activatable cell penetrating peptides (ACPPs) have been used to monitor MMP activity in tumors and, in principle, can be modified to detect other proteases. We have developed a probe that incorporates the peptide sequence DPRSFL from the proteinase activated receptor 1 (PAR-1) into an ACPP and shown that it is preferentially cleaved by purified thrombin. Active thrombin in serum cleaves DPRSFL–ACPP with >90% inhibition by lepirudin or argatroban. The DPRSFL–ACPP cleavage product accumulated in advanced atherosclerotic lesions in living mice, with 85% reduction in retention upon pre-injection of mice with hirudin. Uptake of the ACPP cleavage product was highest in plaques with histological features associated with more severe disease. Freshly resected human atheromas bathed in DPRSFL–ACPP retained 63% greater cleavage product compared to control ACPP. In conclusion, DPRSFL–ACPP can be used to study thrombin activity in coagulation and atherosclerosis with good spatial and temporal resolution. Thrombin-sensitive ACPPs may be developed into probes for early detection and intraoperative imaging of high risk atherosclerotic plaques.

[a] *Department of Pharmacology, University of California at San Diego, La Jolla, CA 92093-0647, USA*
[b] *Medical Scientist Training Program, University of California at San Diego, La Jolla, CA 92093-0647, USA*
[c] *Department of Chemistry and Biochemistry, University of California at San Diego, La Jolla, CA 92093-0647, USA*
[d] *UCSD School of Medicine, University of California at San Diego, La Jolla, CA 92093-0647, USA*
[e] *Howard Hughes Medical Institute, University of California at San Diego, La Jolla, CA 92093-0647, USA*
[f] *Department of Pathology, University of California at San Diego, La Jolla, CA 92093-0647, USA*
[g] *Department of Medicine, University of California at San Diego, La Jolla, CA 92093-0682, USA*
[h] *Division of Otolaryngology-Head and Neck Surgery, University of California at San Diego, La Jolla, CA 92093-0647, USA.*
 E-mail: quyennguyen@ucsd.edu; Fax: +1 858 534-5270; Tel: +1 858 822-3965
† Electronic supplementary information (ESI) available. See DOI: 10.1039/c2ib00161f

Insight, innovation, integration

We have developed a novel activatable probe (ACPP) that can be used as a sensitive *in vivo* thrombin activity sensor. Following systemic injection of a fluorescently-labeled probe, atherosclerotic plaques in transgenic hypercholesterolemic mice accumulate fluorescence. Fluorescence intensity correlates with total plaque burden, histologic grade for a given aorta and is largely abolished with preinjection of direct thrombin inhibitors. Fluorescence also accumulates in human atheromas *ex vivo*. We believe that eventual clinical use of this fluorescently-labeled probe as an *in vivo* thrombin activity sensor should enable improved diagnosis and management of atherosclerosis. We believe that thrombin-sensitive ACPPs will eventually target magnetic resonance imaging contrast agents to atherosclerotic plaques for noninvasive whole-body detection, just as MMP-sensitive ACPPs have enabled molecularly targeted MRI of tumors.

Introduction

Atherosclerotic disease and its complications are among the leading causes of mortality and morbidity in Western society.[1] There are many predictive classification schemes and imaging technologies for morphological classification of atherosclerotic plaques based on histopathology,[2] plaque thickness and hypo-echogenicity on ultrasound,[3,4] anatomical imaging with CT and MRI,[5,6] the presence or absence of lipid laden macrophages.[7] Matrix metalloproteinases (MMPs) and cathepsins have been investigated as *in vivo* biochemical markers of plaque instability and risk of rupture.[8–10] In addition to these enzymes, thrombin may play a role in plaque development and stability as expression and activation of coagulation proteases vary throughout plaque initiation, stabilization and rupture.[11,12] Thrombin, acting through its G-protein coupled receptor PAR-1, is a key component in a wide range of vascular and extravascular disease processes throughout the body, including cancer,[13] cardiovascular diseases,[14,15] acute kidney injury,[16] and stroke.[17] PAR-1 is activated by cleavage of amino acids 39–44 (DPRSFL), mostly by thrombin[18] but to a lesser extent by plasmin,[18–20] trypsin and factor Xa.[20]

There are currently several molecular imaging strategies and reagents available for non-invasive detection of atherosclerosis including MMP sensitive agents such as fluorescent and radio-active MMP inhibitors,[21,22] MMP-cleavable activatable cell penetrating peptides (ACPPs),[23–26] and MMP-cleavable fluorescence dequenching probes.[27] The presence of active MMPs in atheromas *in vivo* has been demonstrated using many of these probes, with some indication that MMP activity correlates with the presence of plaque-associated macrophages.[8,28] Molecular imaging agents have also been designed to detect end stage disease and thrombosis, including ^{99m}Tc-apcitide for platelet glycoprotein IIb/IIIa receptor and EP-2104R for fibrin burden, and many of these are currently being evaluated clinically.[29] Although thrombin has been implicated in a variety of plaque progression and destabilization events[12] a limitation in sorting through the myriad of potential roles for thrombin in atherosclerotic progression is the paucity of tools to spatially localize active thrombin in intact plaques *in vivo*. The feasibility of imaging thrombin activity in clot formation was established by a pioneering study that developed a near-infrared thrombin-activatable dequenching probe[30,31] but the use of these probes in atherosclerosis has not been reported. To study thrombin activation in atherosclerotic plaques, we have designed an ACPP with a cleavage site selective for thrombin (DPRSFL–ACPP). ACPPs are hairpin shaped molecules comprising a polycation (typically 9-D-arginines) and a polyanion (typically 9-D-glutamates) separated by a protease cleavable linker. Cleavage of the linker frees the polycation to associate with cell membranes or the extracellular matrix (Fig. 1A). This mechanism of cleaved product retention distinguishes this class of protease-activatable sensors from fluorescent dequenching probes.[30–32] We have previously studied ACPPs responsive to extracellular enzymes such as MMP-2/-9[23–26] and elastase[33] and have found them to be good reporters for enzymatic activity *in vitro* and *in vivo*. Here, we use this novel thrombin cleavable ACPP to detect thrombin activity in atherosclerotic plaques in mice and compare labeling with our previously described MMP-cleavable ACPP.

Materials and methods

Peptide synthesis

Peptides were synthesized and labeled with Cy5 or rhodamine as previously described.[23] Briefly, peptides were synthesized in an automatic peptide synthesizer following standard procedures for fluorenylmethoxycarbonyl solid-phase synthesis. Peptides were N-terminally capped with a succinate and C-termini were amidated. After cleavage of the resin, the C-termini were labeled through the cysteine with Cy5 or rhodamine monomaleimide. Peptides were purified using HPLC. Specific peptide compositions were: DPRSFL–ACPP = (Suc-e8-O-DPRSFL-r9-c(Cy5 or rhodamine)-CONH$_2$), and mPEG–ACPP = (Suc-e8-(mPEG)-r9-c(Cy5)-CONH$_2$) where O = 5-amino-3-oxapentanoyl and mPEG = –[NH(CH$_2$CH$_2$O)$_2$CH$_2$CO]$_2$–. Lower case letters represent D-amino acids.

Determination of k_{cat}/K_m

Reaction mixtures containing 50 nmol L^{-1} thrombin and seven peptide concentrations ranging from 1 to 30 μmol L^{-1} DPRSFL–ACPP peptide were incubated for 5, 15, 30 and 60 minutes in 100 μL reaction volumes before undergoing tricine gel electrophoresis. Reactions were stopped by addition of SDS containing sample buffer at the appropriate time point. Percent cleavage was assessed as before, and was multiplied by the starting concentration for each vial to obtain the total product concentration. The velocity of each reaction was obtained by determination of the slope of the linear portion of the curve on a scatter plot comparing product *vs.* time. The k_{cat} and K_m were obtained by determining the y-intercept and slope on a Lineweaver–Burke plot.

Enzyme and serum cleavage

Enzymes were obtained commercially: plasmin, factor VIIa, trypsin, chymotrypsin, thrombin, factor XIa, factor XIIa, cathepsin G, neutrophil elastase, and activated protein C (APC) from EMD, La Jolla CA, factor Xa from NEB, Ipswitch, MA, pancreatic elastase from Sigma Aldrich. 5 μmol L^{-1} peptide was incubated with 50 nmol L^{-1} enzyme and the rate of cleavage was determined by the emergence of a lower molecular weight band in tricine gel electrophoresis (Invitrogen). Band intensity was quantified using Image J, with "background" defined as the average of a larger area in the middle of the gel, away from any fluorescence bands. Percent cleavage was defined as (intensity of the lower molecular weight band minus "background")/(intensity of lower plus higher molecular weight band minus 2 times background). To account for minor impurities in the sample, the percent cleavage for an uncleaved substrate has been subtracted off (Fig. S1, ESI†). Whole blood was collected either *via* cardiac puncture or from the abdominal aorta, in either heparinized tubes (plasma) or eppendorf tubes (serum). Both tubes were centrifuged to pellet out the red blood cells, and the supernatant was removed for analysis. Argatroban (Enzo Life Sciences, Plymouth Meeting, PA) and lepirudin (UCSD pharmacy) were used at a final concentration of 4 mg mL^{-1} and 0.5 mg mL^{-1} respectively. After 20 minutes, reactions were stopped by addition of tricine sample buffer, heated to 85 °C and analyzed by gel electrophoresis as above.
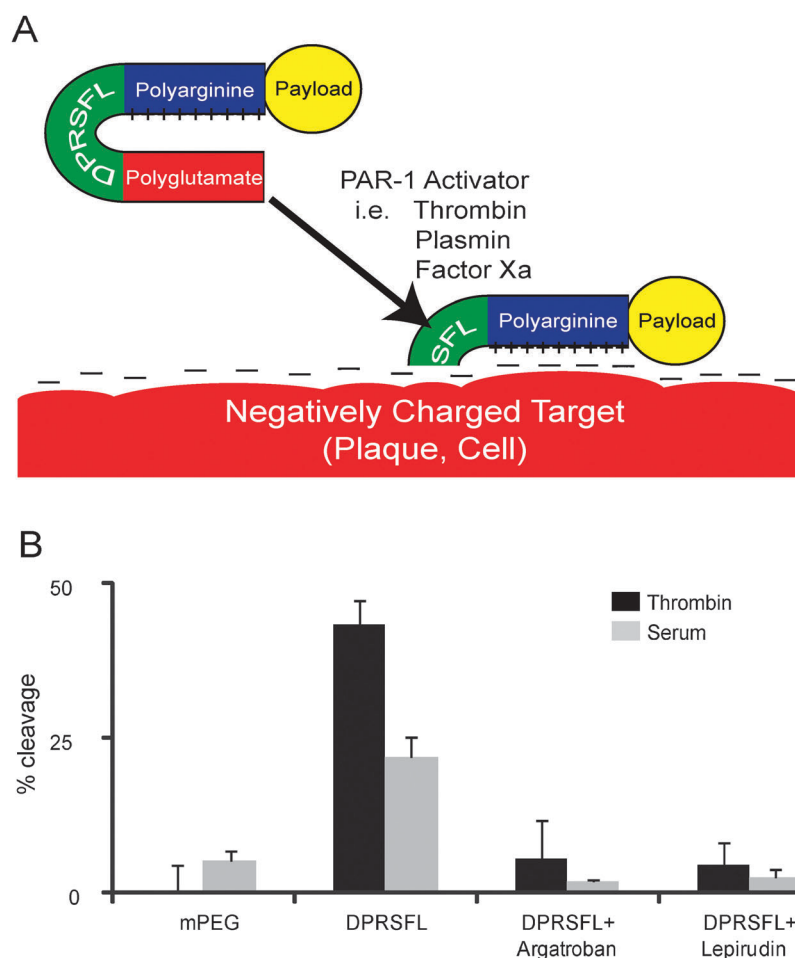
Fig. 1 Protease cleavage of DPRSFL–ACPP is thrombin dependent and promotes uptake of fluorescent payload into cells and plaques. Schematic of an ACPP showing a positively charged polyarginine separated from a negatively charged polyglutamate by DPRSFL, a thrombin cleavable linker derived from the PAR-1 receptor (A). Once the linker is cleaved, the polyarginine is free to associate with negatively charged targets on cellular membranes, within atherosclerotic plaques or other tissue. Analysis of proteolytic cleavage of the DPRSFL–ACPP after 20 minutes incubation at 37 °C with either 50 nM thrombin (dark grey) or 50% mouse serum (light grey) in the presence and absence of the direct thrombin inhibitors argatroban and lepirudin (B) (see Fig. S1A (ESI†) for gel analysis). DPRSFL–ACPP was proteolytically cleaved by both thrombin and serum but not plasma. In each case cleavage was >90% inhibited by either argatroban or lepirudin. Also included are data showing that the negative control mPEG–ACPP is not cleaved by either thrombin or serum. Quantitation of data was done as shown in Fig. S1B (ESI†) and all experiments were done in triplicate.

Animals and preparation of *in vivo* clots

Tails of wildtype FVB mice (Charles River, Wilmington, MA) were clipped 2.5 mm from the tip. Twenty minutes after tail amputation, mice were injected intravenously with 10 nanomoles of either DPRSFL–ACPP or mPEG–ACPP. 24 hours after probe injection, mice were anesthetized with ketamine/midazolam (80 mg kg^{-1}, 5 mg kg^{-1}) and clots at the end of the amputated tail tips were imaged using a Zeiss Lumar dissecting microscope (ex 620/60, em 700/75, 0.8× objective, Zeiss, Peabody, MA). Data were collected using MetaMorph software version 6.1 (Silicon Valley, CA) and quantified using ImageJ software (NIH, Bethesda, MD). Animals were euthanized with isoflurane. Animal procedures were approved by USCD's institutional committee.

Atherosclerosis models

LDLR$^{-/-}$ and ApoE$^{-/-}$ mice were obtained from Jackson. All animals were in a C57/BL6 background backcrossed 10 times.

Mice were fed high cholesterol diet (LDLR$^{-/-}$ = 0.5% and ApoE$^{-/-}$ = 0.15%) for 1–2 years prior to experiments, generating animals with a range of atherosclerotic disease severity.[34]

Ex vivo epifluorescence imaging of aortas

Animals were injected with mPEG–ACPP or DPRSFL–ACPP with or without pre-injection of inhibitor. Inhibitors were recombinant hirudin (2000 U per mouse, EMD Biosciences), or a cocktail of SB3CT (500 µg per animal) and GM6001 (2 mg per animal). Animals were euthanized six hours after injection with ACPP to allow washout of uncleaved probes, then transcardially perfused with saline followed by sucrose buffered formalin. Whole aortas were dissected and pinned open for fluorescence imaging (Maestro™, 700 nm, ex 640/48) (CRI, Woburn MA). Percent plaque and plaque intensity were calculated using Amira software (Visage Imaging, La Jolla, CA), Fig. S1 (ESI†). Plaque intensity is reported as raw

plaque intensity/phantom intensity taken on the same day (Labsphere certified reflectance standard, North Sutton, NH).

Intravital imaging of carotid plaques

Six hours after intravenous injection of ACPPs, animals were anesthetized, the carotid artery was exposed and images were taken using a customized fluorescence dissecting microscope (Olympus MVX). Other structures including the carotid bifurcation and the aortic arch were exposed postmortem and were imaged using a fluorescence dissecting microscope (Zeiss Lumar ex 560/25, em 607/36 for rhodamine, ex 620/60, em 700/75 for Cy5, 0.8× objective, Zeiss, Peabody, MA). After imaging, tissue was frozen on dry ice for histology. Blood half life was determined by serially collecting and imaging 10–20 μL blood in a capillary tube.

Histologic analysis of plaques

Plaque samples were collected and cryoprotected in 30% buffered sucrose. Samples were frozen in Tissue-Tek embedding medium (Torrance CA). Each block was sectioned at 10 micrometres thickness and sections were thaw mounted onto glass slides; adjacent slides were stained with hematoxylin–eosin (H–E) or with the Gomori Trichrome method, coverslipped and imaged using standard light microscopy. Sections were analyzed by a board certified pathologist (SB) who was blinded to all treatment conditions and gross aorta fluorescence. Sections were grouped into two categories based on pathological signs: Group 1 plaques were less advanced and demonstrated a thick, intact smooth muscle cap and few inflammatory cells; Group 2 plaques were more advanced and displayed features associated with vulnerability such as a thin relatively attenuated smooth muscle layer in the plaque cap, infiltrating inflammatory cells, expansion or fissuring of the elastic lamina in the media of the vessel wall. These group assignments were used to sort the fluorescence data of whole aortas for each experimental group (DPRSFL–, PLGLAG– and mPEG–ACPP) and analyzed using Student's t-test (2-tailed, unpaired).

Fluorescence imaging of serial sections was done using the Zeiss Lumar described above. Intensity was quantified in Image J. Average fluorescence intensities were compared for sectioned plaques assigned to Group 1 or Group 2, based on the pathology slide readings. Significance between groups was determined by Student's t-test (2-tailed, unpaired).

Aortas from five LDLR$^{-/-}$ mice injected with DPRSFL–ACPP were sectioned to determine the distribution of DPRSFL–ACPP. Sections were cut at 10 micrometres and coverslipped with ProLong™ Gold antifade reagent with DAPI (4′,6-diamidino-2-phenylindole). Fluorescence images were acquired using a Zeiss epifluorescence microscope (ex/em 350/470 for DAPI, 620/700 for Cy5). Cell-rich and cell poor regions of the plaque were defined by DAPI staining using Image J. The contours of the DAPI-rich and DAPI-poor regions were transferred to the corresponding Cy5 images. Three sections spaced 100 micrometres apart were analyzed for each mouse. Fluorescence intensities of the cellular and hypocellular regions were compared by Student's t-test (2-tailed, paired). Immunohistostaining for macrophages was performed on sections of LDLR$^{-/-}$ aorta following antigen retrieval by incubation for 48 hours in fluorescein

conjugated-rat monoclonal F4/80 antibody (clone BM8) (Abcam AB 60343) ($n = 3$).

Human specimen

Freshly obtained human carotid endarterectomy specimens (UCSD IRB# 080965) were placed on ice prior to embedding in 0.5% agarose gel and cut into 2 mm sections. Sections were incubated for 1 hour in 10 μmol L^{-1} of either DPRSFL–ACPP, PLGLAG–ACPP or mPEG–ACPP. Two sections were incubated in either 110 or 220 μmol L^{-1} argatroban. Samples were washed six times for 15 minutes with PBS prior to embedding in Cryotec and freezing at −80 °C. 8 μm cryostat sections were cut and mounted onto glass slides. Imaging was done using a Zeiss Lumar microscope (ex 620/60, em 700/75, 0.8× objective, 8× magnification). Data were collected using MetaMorph software version 6.1 (Silicon Valley, CA). Quantification of fluorescence intensity was performed using ImageJ software (NIH, Bethesda, MD). Average background fluorescence and fluorescence intensity were measured and background subtracted (Fig. S1, ESI†). Sections from the same atheroma specimens were used to test cleavable and control ACPPs. Analyses were performed using Student's paired-t-test.

Results

Thrombin efficiently cleaved DPRSFL–ACPP

We first used purified thrombin to determine whether two candidate thrombin cleavage sites would be selective for thrombin once incorporated into the typical ACPP hairpin configuration.[23] The first cleavage site tested, norleucine-TPR, was derived from a screen of fluorogenic substrates for thrombin using a positional scanning library[35] and was minimally cleavable by purified thrombin after insertion into the ACPP hairpin. The second, DPRSFL, is comprised of amino acids 39–44 of the PAR-1 thrombin receptor[20] (Fig. 1A). DPRSFL–ACPP was efficiently cleaved by purified thrombin in vitro (Fig. 1B). Kinetic measurements yielded $k_{cat} = 0.3$ s^{-1}, $K_m = 1.5 \times 10^{-5}$ M^{-1}, from which $k_{cat}/K_m = 2.1 \times 10^4$ M^{-1} s^{-1}. The latter is smaller than $k_{cat}/K_m = 3.6 \times 10^5$ M^{-1} s^{-1} for non-ACPP conjugated DPRSFL,[19] perhaps because inclusion within an ACPP may hinder adoption of the extended conformation required for efficient enzymatic action. Thrombin activity on the native PAR-1 receptor was even more efficient, $k_{cat}/K_m = 7.6 \times 10^6$ M^{-1} s^{-1},[36] perhaps because an exosite on the enzyme docks onto a hirudin-like sequence in the substrate.[19] Several other enzymes, including plasmin, factor Xa, trypsin, activated protein C (APC), are known to cleave the PAR-1 receptor in vitro, albeit less efficiently than thrombin. We tested these enzymes in addition to some related proteases for their ability to cut DPRSFL–ACPP. Thrombin, plasmin, trypsin, chymotrypsin, and factor Xa were able to cleave DPRSFL–ACPP, whereas factors VIIa, XIa, XIIa, cathepsin G, neutrophil elastase, and APC showed no cleavage of this peptide (Fig. S1, ESI†). Active serum (but not plasma) also rapidly cleaved DPRSFL–ACPP (Fig. 1B). This proteolysis was inhibited by >90% with direct thrombin inhibitors lepirudin and argatroban, suggesting that thrombin was the dominant protease acting on the DPRSFL–ACPP in this complex mixture of coagulation

enzymes. No proteolysis was seen upon incubation of the DPRSFL–ACPP in anticoagulated blood lacking active thrombin. To verify that DPRSFL–ACPP can detect thrombin activation during *in vivo* blood coagulation, tail tips of wild type mice were amputated prior to injection with either DPRSFL– or mPEG–ACPP. Thrombin cleavable ACPP showed a 2.4 fold increase in fluorescence intensity compared to the uncleavable mPEG–ACPP (533 ± 3, $n = 3$ for DPRSFL–ACPP; 222 ± 118, $n = 3$ for mPEG–ACPP, $p = 0.045$). These results are consistent with previously described thrombin cleavable probes in a similar model.[30]

DPRSFL–ACPP fluorescence uptake in mice correlated with total plaque burden was thrombin dependent

The roles of MMP-2/-9 and thrombin in atherosclerosis were studied in 1–2 year old transgenic mice deficient in either ApoE (ApoE$^{-/-}$) or LDLR (LDLR$^{-/-}$) and maintained on a prolonged high-cholesterol diet (0.5% for LDLR$^{-/-}$ and 0.15% for ApoE$^{-/-}$). Mice were injected intravenously either with DPRSFL–ACPP (Fig. 2A, $n = 17$), DPRSFL–ACPP with pre-injection of hirudin (Fig. 2B, $n = 9$), a previously characterized MMP-2 and -9 cleavable ACPP (PLGLAG–ACPP)[23–25] (Fig. 2C, $n = 12$) or a negative control mPEG–ACPP (Fig. 2D, $n = 11$). The mPEG–ACPP was chosen because it could act as a control for both the PLGLAG–ACPP and the DPRSFL–ACPP.[25] Animals

were euthanized 6 hours after probe injection to allow washout of uncleaved DPRSFL–ACPP (whole blood half-life of 17 ± 5 minutes). Fluorescence uptake was determined by quantitative comparison of the average fluorescence intensity per pixel within whole mount plaque regions from whole dissected aortas (Fig. 2; Fig. S1C and S2, ESI†). Aortas were stratified based on their overall plaque burden as defined by the percentage of imaged whole aorta that displayed gross plaque under white light illumination. Both DPRSFL–ACPP ($n = 17$) and PLGLAG–ACPP ($n = 12$) showed fluorescence uptake that positively correlated with total plaque burden, correlation coefficient 0.82 and 0.90 respectively (Fig. 2E; Fig. S2E, ESI†). The slope of this line ($m = 0.31$ with 95% confidence interval [0.19, 0.43]) was higher for DPRSFL–ACPP than the slope (0.15 with 95% confidence interval [0.10, 0.21]) for PLGLAG–ACPP, but the difference was not statistically significant due to relatively high variation for the DPRSFL probe. Both slopes were significantly greater than that of the mPEG–ACPP ($n = 11$, $m = 0.05$, 95% confidence interval [0.03, 0.08]), and the slope of the line for DPRSFL–ACPP was significantly reduced upon addition of the direct thrombin inhibitor hirudin ($n = 9$, $m = 0.06$, 95% confidence interval [−0.04, 0.17]). PLGLAG–ACPP uptake was reduced by 30% in the presence of MMP-selective inhibitors (GM6001 and SB3CT) in animals with comparable plaque burden ($n = 4$, Fig. 2SE, ESI†).
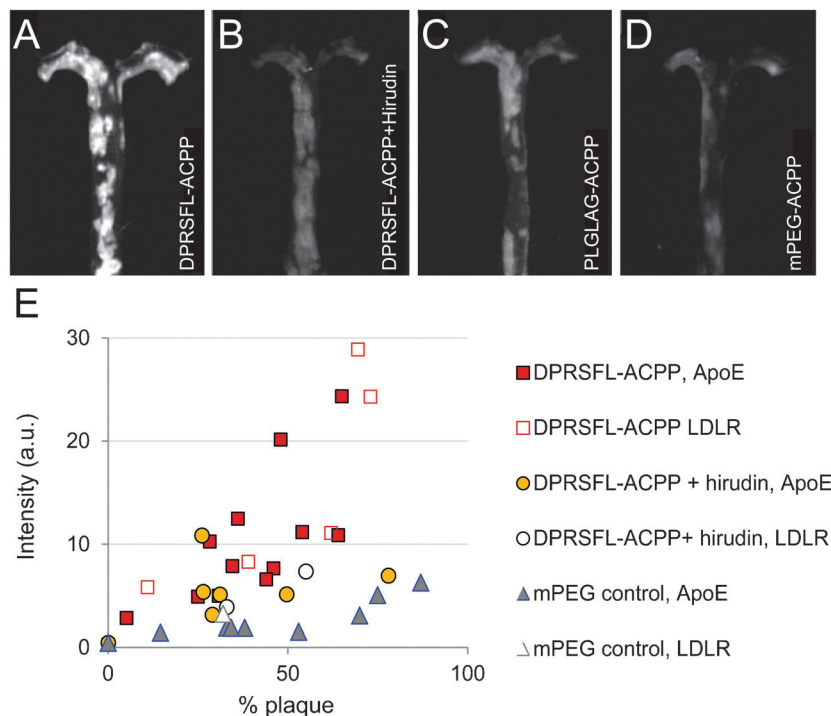

Fig. 2 Fluorescent labeling of atherosclerotic aortas with thrombin or MMP cleavable ACPPs was enzyme dependent and correlated with increased plaque burden. (A–D) Representative fluorescence images are shown of gross aortas that were removed from ApoE$^{-/-}$ animals six hours after injection with either (A) 10 nmol DPRSFL–ACPP ($n = 17 + 1$ wildtype mouse); (B) 10 nmol DPRSFL–ACPP + hirudin ($n = 8 + 1$ wildtype mouse); (C) 10 nmol PLGLAG–ACPP ($n = 11 + 1$ wildtype mouse); (D) 10 nmol control mPEG–ACPP ($n = 9 + 1$ wildtype mouse). Images A–D were acquired and processed using identical parameters. (E) Scatter plot showing average uptake of DPRSFL–ACPP in ApoE (closed shapes) and LDLR (open shapes) deficient mice as a function of plaque burden (quantification of data as shown in Fig. S1C, ESI†). Correlation coefficients for DPRSFL–ACPP, DPRSFL–ACPP + hirudin, PLGLAG–ACPP and mPEG–ACPP were 0.82, 0.48, 0.90 and 0.74 respectively. Slopes and 95% confidence intervals (in brackets) were 0.31 [0.19, 0.43], 0.06 [−0.04, 0.17], 0.15 [0.10, 0.21], 0.05 [0.03, 0.08] respectively.

DPRSFL–ACPP fluorescence uptake in mice is elevated in whole aortas and individual plaques showing features of advanced disease

To correlate histological staging of the aortas with microscopic and gross uptake of the DPRSFL– and PLGLAG–ACPP, single representative plaques from each individual aortic arch were sectioned and stained with hematoxylin–eosin (H–E) and Gomori trichrome. Individual sections were classified into two groups by a board-certified pathologist blinded to the fluorescence measurements. The groups were determined based on the presence of qualitative features associated with plaque progression such as attenuation and thinning of the fibrous cap, presence of acute inflammatory cells and/or hemorrhage and thrombi.[34,37–39] The majority of sectioned-plaques fell into Group 1 ($n = 23/32$, 72%) with features similar to stable/fibrous plaques (Fig. 3A and B). A minority ($n = 9/32$, 28%) of the

Fig. 3 DPRSFL–ACPP uptake in LDLR$^{-/-}$ mouse plaques correlates with histologic features that are suggestive of more advanced disease based on human studies. Representative plaques were taken from each aorta. Serial sections stained with Gomori trichrome (A and B, D and E), black arrow points to nuclei of spindle shaped smooth muscle cells in Group 1 (B) which are reduced or absent in Group 2 (E). Scale bar = 50 micrometres. Sections were then grouped based on thickness of the smooth muscle cap and the presence or absence of neutrophils and other inflammatory cells by a pathologist blinded to the experimental groups. Fluorescent labeling of representative plaques from Groups 1 and 2 is shown in C and F. These groups were analyzed by examining the average fluorescence intensity of whole aortas (G) or sectioned plaques (H) on per pixel basis. Results were analyzed by unpaired Student's t-test, with p-values shown.

plaques was assigned to Group 2 (Fig. 3D and E) with features resembling more advanced disease. No plaques showed signs of hemorrhage or thrombi formation. Plaque samples for Groups 1 and 2 (Fig. 3) illustrate the qualitative differences between these two groups, which are especially apparent in the plaque exterior (compare Fig. 3B and E). The two groups were used to re-analyze gross whole aorta (Fig. 3G) and individual plaque (Fig. 3H) fluorescence intensity. There was little difference between the Group 1 and Group 2 whole aorta fluorescence in animals injected with PLGLAG–ACPP or with mPEG–ACPP. In contrast, for the animals injected with DPRSFL–ACPP, whole aorta fluorescence per pixel was greater in the aortas with sections assigned to Group 2 (24.4 ± 3.6, $n = 4$) than for those with sections assigned to Group 1 (7.8 ± 3.0, $n = 12$, $p = 0.02$). Analyses of fluorescence intensity for individual plaques (Fig. 3C, F, and H) showed similar results (43.7 ± 7.5, $n = 3$ for Group 2 vs. 17.0 ± 9.3, $n = 11$ for Group 1, $p = 0.007$).

DPRSFL–ACPP preferentially accumulates within the fibrous layer of atheromas from LDLR deficient mice

LDLR deficient mice are notable for their relatively simple atherosclerotic plaque structure,[40,41] with plaques comprised of a superficial region enriched in fat-laden macrophages and capsular smooth muscle cells, and high levels of MMP-2/-9 activity.[42,43] The deeper hypocellular region was comprised largely of collagen and other extracellular matrix proteins.[41] Most of the DPRSFL uptake was localized in the deep part of the intima, as illustrated in two morphologically distinct plaques. Conversely, little DPRSFL uptake was observed in relation to the foam cells (Fig. 4A) or the smooth muscle cells (Fig.4D) that populate the superficial part of each plaque. For quantification, masks of cell rich and poor regions were drawn on the basis of DAPI nuclear staining (Fig. 4E) which distinguishes regions with numerous nuclei in the superficial plaque from hypocellular fibrous regions in the plaque core. Using this analysis we were able to determine that the uptake of Cy5-DPRSFL fluorescence (Fig. 4C and F) was statistically greater in the hypocellular (DAPI poor) region versus the cellular rich exterior (Fig. 4G) (15 plaques; $p = 0.023$, paired two tailed Student's t-test).

DPRSFL–ACPP fluorescence uptake into ex vivo human atheromas was thrombin dependent

Because extensive preclinical development and regulatory approval will be required before any injection of ACPPs into patients, human plaques can only be tested ex vivo at this stage. Human atheroma specimens were obtained from five patients undergoing carotid endarterectomy. Since this ex vivo tissue lacks intact vasculature, each specimen was cut into 2 mm thick slices to facilitate access and washout of ACPP. These slices were incubated in either Cy5-labeled DPRSFL–ACPP, PLGLAG–ACPP or mPEG–ACPP. For analysis, each slice was cryosectioned and fluorescence uptake measured (Fig. 5A–C). H–E staining confirmed that all of the plaques removed were at least AHA class 5 fibroatheroma (Fig. 5D). Cryosections of slices from atheromas incubated with DPRSFL–ACPP showed increased fluorescent labeling compared to
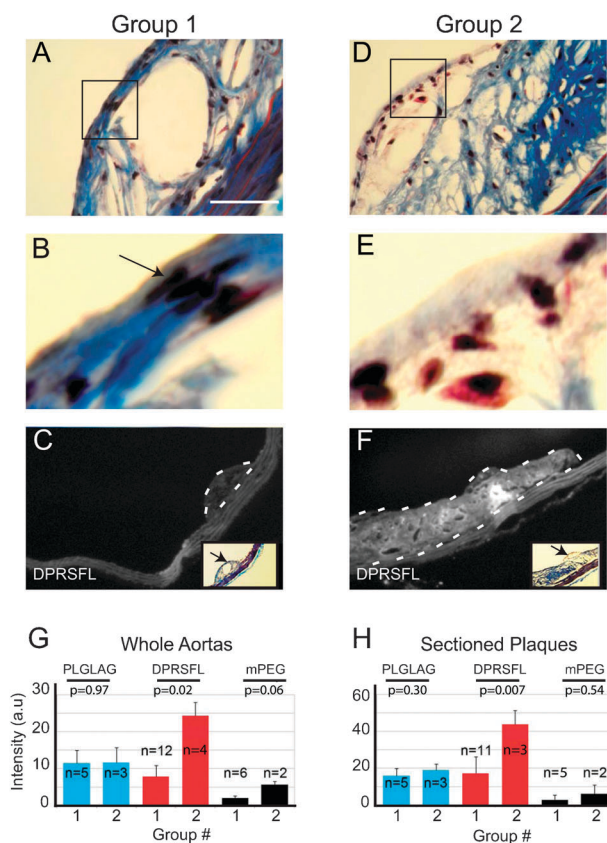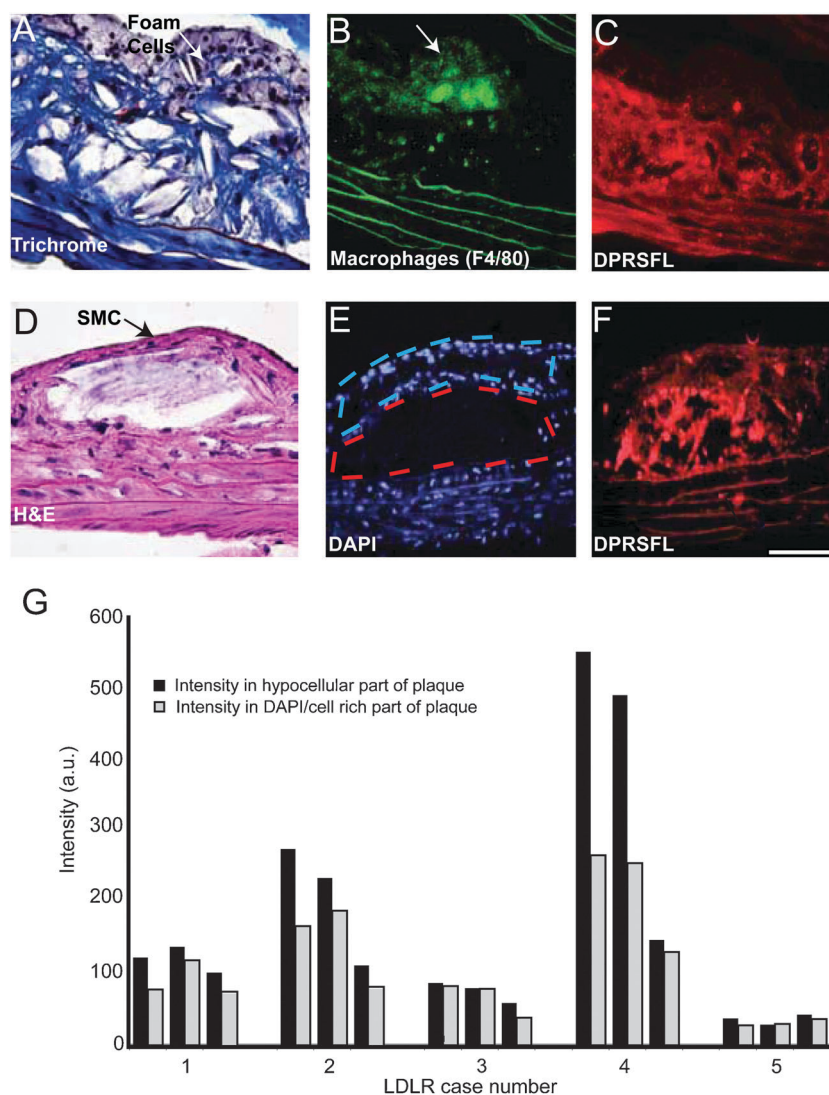
Fig. 4 Thrombin activity, detected by DPRSFL–ACPP labeling, is localized in the deeper fibro-collagenous region of plaque and away from the foam cells. (A–F) Adjacent sections (A–C) from one plaque and (D–F) from another plaque from LDLR$^{-/-}$ mice. Trichrome (A) and H–E (D) staining show an interior core of fibrous tissue and a superficial layer of foam/smooth muscle cells. Macrophage identity was confirmed by F4/80 staining and coincided with the superficial foam cell layer (B). Cy5 uptake resulting from cleavage of DPRSFL–ACPP is localized primarily to the deeper fibrous layer (C,F). The histological sections (A,D) highlight the finding that although these two representative plaques are distinct in their morphology, they both show a similar localization of DPRSFL–ACPP fluorescence within the interior/deeper neointima of the plaques. Sections were stained with DAPI to differentiate the nucleus-rich foam cells/smooth muscle cell layer with nucleus-poor interior fibrous layers (E). This information was used to quantify the differential Cy5–DPRSFL–ACPP distribution ($n = 5$ mice, three sections collected at 100 micrometre intervals per mouse, G). $p = 0.02$, Student's t-test, 2 tailed paired (scale bar: A,D = 60 micrometres, C,D and E,F = 100 micrometres).

similar sections from the same atheroma incubated in either PLGLAG–ACPP (3.1 ± 0.8 ($n = 5$) vs. 1.7 ± 0.6 ($n = 5$), $p = 0.03$ by matched pairs Student's t-test) or mPEG–ACPP (1.9 ± 1.1 ($n = 5$), $p = 0.009$ by matched pairs Student's t-test) (Fig. 5E). For two atheroma specimens where there was sufficient material to incubate a separate slice in an ACPP with inhibitor, fluorescence intensity of cryosections incubated with DPRSFL–ACPP in the presence of argatroban showed a $76.6 \pm 13.4\%$ reduction in fluorescence intensity relative to DPRSFL–ACPP alone. After incubation, the slices were homogenized in SDS sample buffer, centrifuged and the supernatants were analyzed by gel electrophoresis. We found that

human atheromas cleaved DPRSFL–ACPP but not the control mPEG–ACPP (Fig. 5F).

DPRSFL–ACPP fluorescence uptake in living animals

In the previous animal experiments, the *in vivo* uptake of DPRSFL–ACPP was imaged post-mortem in fully exposed plaques or atheromas to allow high resolution analysis and validation. A complementary application of DPRSFL–ACPP would be to visualize more advanced plaques during carotid endarterectomies where disruption of plaques at the time of surgery places patients at increased risk for cerebrovascular accidents.[44]
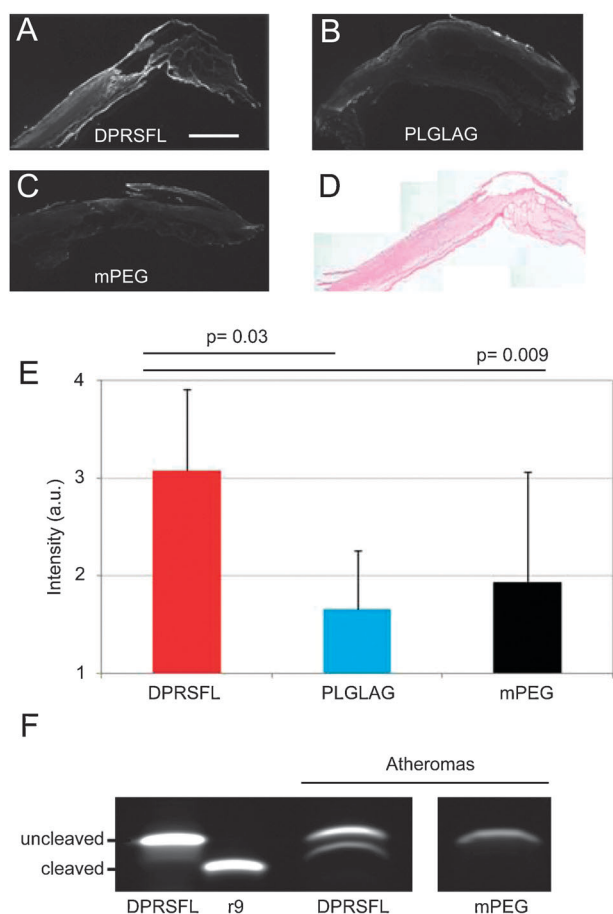
Fig. 5 DPRSFL–ACPP highlights thrombin activity in a resected human carotid endarterectomy specimen. Fluorescence micrographs showing serial sections of a single atheroma incubated in DPRSFL–ACPP (A), PLGLAG–ACPP (B) or mPEG–ACPP (C). All of the atheromas tested were AHA Class 5 by H–E stain (D). (E and F) Combined average intensities of seven representative sections from each of the treatment groups, with statistical significance assessed by paired Student's *t*-test (E). Gel electrophoresis confirming cleavage of the DPRSFL–ACPP but not the control mPEG–ACPP in homogenized carotid tissue which had been pre-treated with peptide. The molecular weight of the cleaved product is approximated by r9 (F).

To assess the feasibility of such an approach and more specifically the suitability of thrombin as an enzymatic target, we examined plaque laden arteries in high risk areas such as the carotid bifurcation in living (Fig. 6A and B) and freshly euthanized mice (Fig. 6C–J). Imaging through the vessel walls revealed fluorescent regions in the ascending common carotid artery and carotid bifurcation that corresponded microscopically to atherosclerotic plaque in nearly occluded vessels (Fig. 6C–E). Post-mortem cross-sections through these macroscopically fluorescent regions confirmed uptake of DPRSFL–ACPP into plaques (Fig. 6D and E). Neighboring regions showed minimal uptake into the vessel wall in the absence of plaques (Fig. 6F and G). Finally, in two animals coinjected with rhodamine–DPRSFL–ACPP and Cy5–PLGLAG–ACPP, DPRSFL–ACPP uptake (Fig. 6H) was much higher than that of PLGLAG–ACPP (Fig. 6I) within the same atherosclerotic plaques. A cross section of the common carotid artery just below the bifurcation is shown

in Fig. 6J, confirming the presence of near occlusive plaque. The same animal had plaques in the coronary artery that also displayed high uptake of DPRSFL–ACPP (Fig. S3, ESI†).

Discussion

In this manuscript, we show a novel ACPP that can detect *in vivo* thrombin activity. The mechanism of ACPP activation and binding has been previously described for MMP cleavable probes in cancer. Upon cleavage by thrombin, the released CPP portion with attached fluorescent label binds to immediately neighboring tissue and cells, resulting in robust anatomical delineation of *in vivo* thrombin activity. The data presented here suggest a correlation between elevated thrombin activity and histologic features associated with atherosclerotic plaques of more advanced disease. A robust *in vivo* sensor that differentially highlights plaques at varied stages of disease would be useful in both diagnosis and treatment of disease. For example, fluorescently labeled DPRSFL–ACPP presented here, in conjunction with intraoperative fluorescence imaging,[45] could be used during surgery to highlight atherosclerotic plaques from outside the vessel wall during coronary artery bypass grafting or carotid endarterectomy to avoid inadvertent disruption of plaques intraoperatively.[44]

Our studies with the DPRSFL–ACPP raise some intriguing possibilities with regard to whole animal plaque imaging. While the current work was done with a free peptide ACPP conjugated to Cy5 to show proof-of-principle that the thrombin cleavable ACPP could detect intravascular plaque under physiologic blood flow, thrombin cleavable ACPPs could be attached to NIRF fluorochromes such as Cy7 or AF750 for whole body fluorescence tomography,[46] or large molecular weight nanoparticles loaded with gadolinium for MRI just as MMP cleavable ACPPs have been used in cancer models.[26]

A persistent challenge for protease cleavable probes is specificity. Using hirudin, a direct and specific thrombin inhibitor, we showed that DPRSFL–ACPP is selective for thrombin *in vivo*. The fluorescence intensity as a function of the plaque burden slope changed from 0.31 to 0.06 with hirudin pretreatment, implying nearly 80% specificity. This *in vivo* selectivity, despite its *in vitro* susceptibility to other enzymes such as plasmin and factor Xa, may be partially explained by the varied plasma concentrations of the proenzymes (1.4 μmol L^{-1} for pro-thrombin, 170 nmol L^{-1} for factor X[47] and 62 μmol L^{-1} for plasminogen) and the presence of regulator inhibitors such as antithrombin and antiplasmin.[48] The selectivity of the PLGLAG sequence for MMP-2 and -9 has been previously described for tumors.[23–25] We did note decreased efficacy of the MMP inhibitor cocktail in this study relative to results presented previously[25] which suggests that non-MMP proteases may contribute a greater percentage of PLGLAG–ACPP cleavage in atheromas than in tumors. An advantage of ACPP-based imaging agents over previously described near-infrared thrombin-activatable dequenching probes[30,31] is that there is a mechanism for retention of the cleaved product at the site of activation, allowing for the possibility of imaging with MRI.[26,49]

We found that histologically, fluorescence uptake of our probe is highest in the subendothelial, matrix rich parts of plaque, a localization consistent with previous reports of thrombin antibody
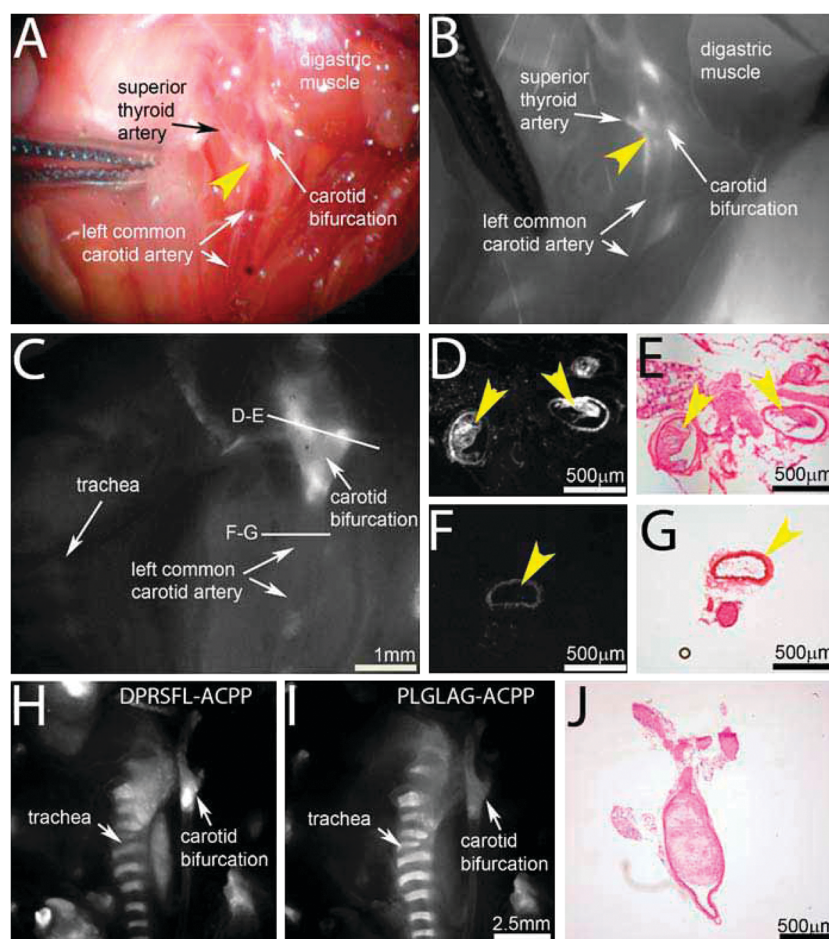
Fig. 6 DPRSFL–ACPP highlights plaques in the carotid arteries of LDLR$^{-/-}$ mice. (A and B) Brightfield (A) and Cy5 fluorescence (B) images of carotid plaques in a living mouse six hours after injection with 10 nmol DPRSFL–ACPP. Plaque barely visible in the reflected white light intraoperative image (A—yellow arrowhead) is highlighted in the fluorescence image at the level of the carotid bifurcation (B—yellow arrowhead). (C–G) Fluorescence images taken postmortem of a similar animal following a more extensive surgical exposure of the carotid bifurcation is shown in (C). From this specimen, vessels with (D and E) and without (F and G) highlighted plaques were taken for sectioning and Cy5 fluorescence imaging (D and F). H–E staining confirmed the presence (E) and absence (G) of plaques within the vessel lumen (yellow arrowheads). (H–J) Similar fluorescence images of a mouse injected with both rhodamine–DPRSFL–ACPP (H) and Cy5–PLGLAG–ACPP (I) showing improved delineation of the plaque area at the level of the carotid bifurcation with rhodamine–DPRSFL–ACPP (H). An H–E cross-section (J) near the carotid bifurcation verified near occlusion of the same carotid artery as in (H and I).

binding in human atheromas.[50] Interestingly, thrombin in this location has also been shown to colocalize with plasminogen activator inhibitor 1 (PAI-1) and vitronectin.[50] A second advantage is that the DPRSFL–ACPP targets protease activity deep in the atherosclerotic plaques, a region that is distinct to that seen with MMP based probes or probes targeting macrophages.[7,42] Efforts are ongoing to improve the selectivity and kinetics of both thrombin and MMP-cleavable ACPPs with sequence variations and conjugation to high molecular weight carriers.

The ability to image total plaque burden can be effectively evaluated with MRI or ultrasound for carotids and CTA for coronary arteries. However, these current imaging modalities do not allow staging/differentiation of severe plaques from lower stage/stable plaques. The finding that fluorescence uptake of our probe correlates with histologic features of plaques that have been associated with more advanced disease in human studies[2,39] raises the possibility that our probe may be

able to detect plaques at high risk of rupture. This information distinguishes potentially stable plaques from plaques that may be at risk of rupture and is important in the evaluation and management of patients with atherosclerotic disease. The mice used in this study have plaques that exhibit histologic features similar to those described for advanced plaques in prior studies of older animals.[51] This study used animals that had evidence of very advanced atherosclerosis in order to evaluate the ability of DPRSFL–ACPP to differentiate between more or less advanced disease. The advanced age of the animals and high total plaque burden required for this study limited the total number of animals available. Nevertheless, the number of animals was adequate to reach statistical significance supporting key conclusions. Longitudinal studies will be needed to determine whether thrombin activating plaques are responsible for sudden cardiac death and intramural thrombi previously reported in mice.

Conclusions

In this study, we showed selective accumulation of a novel fluorescently labeled ACPP targeting thrombin activity within vulnerable atherosclerotic plaques of hypercholesterolemic transgenic mice. Higher fluorescence intensity was detected with increased total plaque burden and plaques with histologic features similar to those found in high-risk human atherosclerotic disease. Finally, a novel fluorescently labeled thrombin-selective ACPP was used to image atherosclerotic plaques in living mice under conditions of normal blood flow and in freshly resected human atheromas. This finding suggests that it may be reasonable to test our probe in larger animal models of atherosclerosis by imaging through arterial blood (arterial lumen) *via* a catheter that can deliver and collect light under physiologic blood flow.[52] Ongoing studies are focused on designing thrombin cleavable ACPPs for non-invasive tomographic imaging modalities.

Non-standard abbreviations and acronyms

ACPP	Activatable cell penetrating peptide
DPRSFL	The peptide sequence "Aspartate-proline-arginine-serine-phenylalanine-leucine"
CT	Computerized tomography
MRI	Magnetic resonance imaging
MMP	Matrix metalloproteinase
PAR-1	Proteinase activated receptor
PEG	Polyethylene glycol
HPLC	High performance liquid chromatography
APC	Activated protein C
SDS	Sodium dodecyl sulfate
LDLR	Low density lipoprotein receptor
ApoE	Apolipoprotein E
DAPI	4′,6-Diamidino-2-phenylindole
TPR	Threonine-proline-arginine

Disclosures

ESO, MW, TJ, SB, QTN, TAA and RYT have consulting agreements with Avelas Biosciences.

References

1 V. L. Roger, A. S. Go, D. M. Lloyd-Jones, E. J. Benjamin, J. D. Berry, W. B. Borden, D. M. Bravata, S. Dai, E. S. Ford, C. S. Fox, H. J. Fullerton, C. Gillespie, S. M. Hailpern, J. A. Heit, V. J. Howard, B. M. Kissela, S. J. Kittner, D. T. Lackland, J. H. Lichtman, L. D. Lisabeth, D. M. Makuc, G. M. Marcus, A. Marelli, D. B. Matchar, C. S. Moy, D. Mozaffarian, M. E. Mussolino, G. Nichol, N. P. Paynter, E. Z. Soliman, P. D. Sorlie, N. Sotoodehnia, T. N. Turan, S. S. Virani, N. D. Wong, D. Woo and M. B. Turner, Executive summary: Heart disease and stroke statistics–2012 update: A report from the American heart association, *Circulation*, 2012, **125**, 188–197.

2 H. C. Stary, A. B. Chandler, R. E. Dinsmore, V. Fuster, S. Glagov, W. Insull, Jr., M. E. Rosenfeld, C. J. Schwartz, W. D. Wagner and R. W. Wissler, A definition of advanced types of atherosclerotic lesions and a histological classification of atherosclerosis. A report from the committee on vascular lesions of the council on arteriosclerosis, American heart association, *Circulation*, 1995, **92**, 1355–1374.

3 M. E. Gaunt, L. Brown, T. Hartshorne, P. R. Bell and A. R. Naylor, Unstable carotid plaques: Preoperative identification and association with intraoperative embolisation detected by transcranial doppler, *Eur. J. Vasc. Endovasc. Surg.*, 1996, **11**, 78–82.

4 A. Cohen, C. Tzourio, B. Bertrand, C. Chauvel, M. G. Bousser and P. Amarenco, Aortic plaque morphology and vascular events: A follow-up study in patients with ischemic stroke. Faps investigators. French study of aortic plaques in stroke, *Circulation*, 1997, **96**, 3838–3841.

5 M. Wintermark, S. S. Jawadi, J. H. Rapp, T. Tihan, E. Tong, D. V. Glidden, S. Abedin, S. Schaeffer, G. Acevedo-Bolton, B. Boudignon, B. Orwoll, X. Pan and D. Saloner, High-resolution ct imaging of carotid artery atherosclerotic plaques, *AJNR Am. J. Neuroradiol.*, 2008, **29**, 875–882.

6 H. R. Underhill, T. S. Hatsukami, Z. A. Fayad, V. Fuster and C. Yuan, Mri of carotid atherosclerosis: Clinical implications and future directions, *Nat. Rev. Cardiol.*, 2010, **7**, 165–173.

7 C. Vinegoni, I. Botnaru, E. Aikawa, M. A. Calfon, Y. Iwamoto, E. J. Folco, V. Ntziachristos, R. Weissleder, P. Libby and F. A. Jaffer, Indocyanine green enables near-infrared fluorescence imaging of lipid-rich, inflamed atherosclerotic plaques, *Sci. Transl. Med.*, 2011, **3**, 84ra45.

8 N. Haider, D. Hartung, S. Fujimoto, A. Petrov, F. D. Kolodgie, R. Virmani, S. Ohshima, H. Liu, J. Zhou, A. Fujimoto, A. Tahara, L. Hofstra, N. Narula, C. Reutelingsperger and J. Narula, Dual molecular imaging for targeting metalloproteinase activity and apoptosis in atherosclerosis: Molecular imaging facilitates understanding of pathogenesis, *J. Nucl. Cardiol.*, 2009, **16**, 753–762.

9 F. A. Jaffer, D. E. Kim, L. Quinti, C. H. Tung, E. Aikawa, A. N. Pande, R. H. Kohler, G. P. Shi, P. Libby and R. Weissleder, Optical visualization of cathepsin *k* activity in atherosclerosis with a novel, protease-activatable fluorescence sensor, *Circulation*, 2007, **115**, 2292–2298.

10 Z. Li, L. Li, H. R. Zielke, L. Cheng, R. Xiao, M. T. Crow, W. G. Stetler-Stevenson, J. Froehlich and E. G. Lakatta, Increased expression of 72-kd type iv collagenase (mmp-2) in human aortic atherosclerotic lesions, *Am. J. Pathol.*, 1996, **148**, 121–128.

11 J. I. Borissoff, S. Heeneman, E. Kilinc, P. Kassak, R. Van Oerle, K. Winckers, J. W. Govers-Riemslag, K. Hamulyak, T. M. Hackeng, M. J. Daemen, H. ten Cate and H. M. Spronk, Early atherosclerosis exhibits an enhanced procoagulant state, *Circulation*, 2010, **122**, 821–830.

12 J. I. Borissoff, H. M. Spronk, S. Heeneman and H. ten Cate, Is thrombin a key player in the 'coagulation-atherogenesis' maze?, *Cardiovasc. Res.*, 2009, **82**, 392–403.

13 M. T. Garcia-Lopez, M. Gutierrez-Rodriguez and R. Herranz, Thrombin-activated receptors: Promising targets for cancer therapy?, *Curr. Med. Chem.*, 2010, **17**, 109–128.

14 E. Aikawa, M. Nahrendorf, J. L. Figueiredo, F. K. Swirski, T. Shtatland, R. H. Kohler, F. A. Jaffer, M. Aikawa and R. Weissleder, Osteogenesis associates with inflammation in early-stage atherosclerosis evaluated by molecular imaging *in vivo*, *Circulation*, 2007, **116**, 2841–2850.

15 A. J. Leger, L. Covic and A. Kuliopulos, Protease-activated receptors in cardiovascular diseases, *Circulation*, 2006, **114**, 1070–1077.

16 A. Gupta, M. D. Williams, W. L. Macias, B. A. Molitoris and B. W. Grinnell, Activated protein c and acute kidney injury: Selective targeting of par-1, *Curr. Drug Targets*, 2009, **10**, 1212–1226.

17 G. Mannaioni, A. G. Orr, C. E. Hamill, H. Yuan, K. H. Pedone, K. L. McCoy, R. Palmini Berlinguer, C. E. Junge, C. J. Lee,

M. Yepes, J. R. Hepler and S. F. Traynelis, Plasmin potentiates synaptic n-methyl-d-aspartate receptor function in hippocampal neurons through activation of protease-activated receptor-1, *J. Biol. Chem.*, 2008, **283**, 20600–20611.

18 A. Kuliopulos, L. Covic, S. K. Seeley, P. J. Sheridan, J. Helin and C. E. Costello, Plasmin desensitization of the par1 thrombin receptor: Kinetics, sites of truncation, and implications for thrombolytic therapy, *Biochemistry*, 1999, **38**, 4572–4585.

19 S. L. Jacques, M. LeMasurier, P. J. Sheridan, S. K. Seeley and A. Kuliopulos, Substrate-assisted catalysis of the par1 thrombin receptor. Enhancement of macromolecular association and cleavage, *J. Biol. Chem.*, 2000, **275**, 40671–40678.

20 M. A. Parry, T. Myles, J. Tschopp and S. R. Stone, Cleavage of the thrombin receptor: Identification of potential activators and inactivators, *Biochem. J.*, 1996, **320**(Pt 1), 335–341.

21 H. J. Breyholz, S. Wagner, A. Faust, B. Riemann, C. Holtke, S. Hermann, O. Schober, M. Schafers and K. Kopka, Radio-fluorinated pyrimidine-2,4,6-triones as molecular probes for non-invasive mmp-targeted imaging, *ChemMedChem*, 2010, **5**, 777–789.

22 A. Faust, B. Waschkau, J. Waldeck, C. Holtke, H. J. Breyholz, S. Wagner, K. Kopka, W. Heindel, M. Schafers and C. Bremer, Synthesis and evaluation of a novel fluorescent photoprobe for imaging matrix metalloproteinases, *Bioconjugate Chem.*, 2008, **19**, 1001–1008.

23 T. A. Aguilera, E. S. Olson, M. M. Timmers, T. Jiang and R. Y. Tsien, Systemic *in vivo* distribution of activatable cell penetrating peptides is superior to that of cell penetrating peptides, *Integr. Biol.*, 2009, **1**, 371–381.

24 T. Jiang, E. S. Olson, Q. T. Nguyen, M. Roy, P. A. Jennings and R. Y. Tsien, Tumor imaging by means of proteolytic activation of cell-penetrating peptides, *Proc. Natl. Acad. Sci. U. S. A.*, 2004, **101**, 17867–17872.

25 E. S. Olson, T. A. Aguilera, T. Jiang, L. G. Ellies, Q. T. Nguyen, E. H. Wong, L. A. Gross and R. Y. Tsien, In vivo characterization of activatable cell penetrating peptides for targeting protease activity in cancer, *Integr. Biol.*, 2009, **1**, 382–393.

26 E. S. Olson, T. Jiang, T. A. Aguilera, Q. T. Nguyen, L. G. Ellies, M. Scadeng and R. Y. Tsien, Activatable cell penetrating peptides linked to nanoparticles as dual probes for *in vivo* fluorescence and mr imaging of proteases, *Proc. Natl. Acad. Sci. U. S. A.*, 2010, **107**, 4311–4316.

27 C. Bremer, S. Bredow, U. Mahmood, R. Weissleder and C. H. Tung, Optical imaging of matrix metalloproteinase-2 activity in tumors: Feasibility study in a mouse model, *Radiology (Oak Brook, IL, U. S.)*, 2001, **221**, 523–529.

28 S. Ohshima, S. Fujimoto, A. Petrov, H. Nakagami, N. Haider, J. Zhou, N. Tahara, M. K. Osako, A. Fujimoto, J. Zhu, T. Murohara, D. S. Edwards, N. Narula, N. D. Wong, Y. Chandrashekhar, R. Morishita and J. Narula, Effect of an antimicrobial agent on atherosclerotic plaques: Assessment of metalloproteinase activity by molecular imaging, *J. Am. Coll. Cardiol.*, 2010, **55**, 1240–1249.

29 F. A. Jaffer, P. Libby and R. Weissleder, Molecular imaging of cardiovascular disease, *Circulation*, 2007, **116**, 1052–1061.

30 F. A. Jaffer, C. H. Tung, R. E. Gerszten and R. Weissleder, *In vivo* imaging of thrombin activity in experimental thrombi with thrombin-sensitive near-infrared molecular probe, *Arterioscler., Thromb., Vasc. Biol.*, 2002, **22**, 1929–1935.

31 C. H. Tung, R. E. Gerszten, F. A. Jaffer and R. Weissleder, A novel near-infrared fluorescence sensor for detection of thrombin activation in blood, *ChemBioChem*, 2002, **3**, 207–211.

32 G. Blum, G. von Degenfeld, M. J. Merchant, H. M. Blau and M. Bogyo, Noninvasive optical imaging of cysteine protease activity using fluorescently quenched activity-based probes, *Nat. Chem. Biol.*, 2007, **3**, 668–677.

33 M. Whitney, J. L. Crisp, E. S. Olson, T. A. Aguilera, L. A. Gross, L. G. Ellies and R. Y. Tsien, Parallel *in vivo* and *in vitro* selection using phage display identifies protease-dependent tumor-targeting peptides, *J. Biol. Chem.*, 2010, **285**, 22532–22541.

34 R. Coleman, T. Hayek, S. Keidar and M. Aviram, A mouse model for human atherosclerosis: Long-term histopathological study of lesion development in the aortic arch of apolipoprotein e-deficient (e0) mice, *Acta Histochem.*, 2006, **108**, 415–424.

35 B. J. Backes, J. L. Harris, F. Leonetti, C. S. Craik and J. A. Ellman, Synthesis of positional-scanning libraries of fluorogenic peptide

substrates to define the extended substrate specificity of plasmin and thrombin, *Nat. Biotechnol.*, 2000, **18**, 187–193.

36 A. Kuliopulos, L. Covic, S. K. Seeley, P. J. Sheridan, J. Helin and C. E. Costello, Plasmin desensitization of the par1 thrombin receptor: Kinetics, sites of truncation, and implications for thrombolytic therapy, *Biochemistry*, 1999, **38**, 4572–4585.

37 R. L. Reddick, S. H. Zhang and N. Maeda, Atherosclerosis in mice lacking apo e. Evaluation of lesional development and progression, *Arterioscler. Thromb.*, 1994, **14**, 141–147.

38 H. C. Stary, A. B. Chandler, S. Glagov, J. R. Guyton, W. Insull, Jr., M. E. Rosenfeld, S. A. Schaffer, C. J. Schwartz, W. D. Wagner and R. W. Wissler, A definition of initial, fatty streak, and intermediate lesions of atherosclerosis. A report from the committee on vascular lesions of the council on arteriosclerosis, American heart association, *Circulation*, 1994, **89**, 2462–2478.

39 G. W. Stone, A. Maehara, A. J. Lansky, B. de Bruyne, E. Cristea, G. S. Mintz, R. Mehran, J. McPherson, N. Farhat, S. P. Marso, H. Parise, B. Templin, R. White, Z. Zhang and P. W. Serruys, A prospective natural-history study of coronary atherosclerosis, *N. Engl. J. Med.*, 2011, **364**, 226–235.

40 S. Ishibashi, J. L. Goldstein, M. S. Brown, J. Herz and D. K. Burns, Massive xanthomatosis and atherosclerosis in cholesterol-fed low density lipoprotein receptor-negative mice, *J. Clin. Invest.*, 1994, **93**, 1885–1893.

41 W. Palinski, R. K. Tangirala, E. Miller, S. G. Young and J. L. Witztum, Increased autoantibody titers against epitopes of oxidized ldl in ldl receptor-deficient mice with increased athero-sclerosis, *Arterioscler., Thromb., Vasc. Biol.*, 1995, **15**, 1569–1576.

42 J. O. Deguchi, M. Aikawa, C. H. Tung, E. Aikawa, D. E. Kim, V. Ntziachristos, R. Weissleder and P. Libby, Inflammation in atherosclerosis: Visualizing matrix metalloproteinase action in macrophages *in vivo*, *Circulation*, 2006, **114**, 55–62.

43 S. Ohshima, A. Petrov, S. Fujimoto, J. Zhou, M. Azure, D. S. Edwards, T. Murohara, N. Narula, S. Tsimikas and J. Narula, Molecular imaging of matrix metalloproteinase expression in atherosclerotic plaques of mice deficient in apolipoprotein e or low-density-lipoprotein receptor, *J. Nucl. Med.*, 2009, **50**, 612–617.

44 F. L. Silver, A. Mackey, W. M. Clark, W. Brooks, C. H. Timaran, D. Chiu, L. B. Goldstein, J. F. Meschia, R. D. Ferguson, W. S. Moore, G. Howard and T. G. Brott, Safety of stenting and endarterectomy by symptomatic status in the carotid revascularization endarterectomy *versus* stenting trial (crest), *Stroke*, 2011, **42**, 675–680.

45 G. M. van Dam, G. Themelis, L. M. Crane, N. J. Harlaar, R. G. Pleijhuis, W. Kelder, A. Sarantopoulos, J. S. de Jong, H. J. Arts, A. G. van der Zee, J. Bart, P. S. Low and V. Ntziachristos, Intraoperative tumor-specific fluorescence imaging in ovarian cancer by folate receptor-alpha targeting: First in-human results, *Nat. Med. (N. Y.)*, 2011, **17**, 1315–1319.

46 D. Razansky, N. Deliolanis, C. Vinegoni and V. Ntziachristos, Deep tissue optical and optoacoustic molecular imaging technologies for small animal research and drug discovery, *Curr. Pharm. Biotechnol.*, 2012, **13**, 504–22.

47 S. Butenas, C. van't Veer and K. G. Mann, "Normal" thrombin generation, *Blood*, 1999, **94**, 2169–2178.

48 S. A. Cederholm-Williams, Concentration of plasminogen and antiplasmin in plasma and serum, *J. Clin. Pathol.*, 1981, **34**, 979–981.

49 Q. T. Nguyen, E. S. Olson, T. A. Aguilera, T. Jiang, M. Scadeng, L. G. Ellies and R. Y. Tsien, Surgery with molecular fluorescence imaging using activatable cell-penetrating peptides decreases residual cancer and improves survival, *Proc. Natl. Acad. Sci. U. S. A.*, 2010, **107**, 4317–4322.

50 A. A. Stoop, F. Lupu and H. Pannekoek, Colocalization of thrombin, pai-1, and vitronectin in the atherosclerotic vessel wall: A potential regulatory mechanism of thrombin activity by pai-1/vitronectin complexes, *Arterioscler., Thromb., Vasc. Biol.*, 2000, **20**, 1143–1149.

51 R. K. Tangirala, E. M. Rubin and W. Palinski, Quantitation of atherosclerosis in murine models: Correlation between lesions in the aortic origin and in the entire aorta, and differences in the extent of lesions between sexes in ldl receptor-deficient and apolipoprotein e-deficient mice, *J. Lipid Res.*, 1995, **36**, 2320–2328.

52 H. Yoo, J. W. Kim, M. Shishkov, E. Namati, T. Morse, R. Shubochkin, J. R. McCarthy, V. Ntziachristos, B. E. Bouma, F. A. Jaffer and G. J. Tearney, *Nat. Med*, 2011, **17**, 1680–4.